Clays and Clay Minerals, Vol. 53, No. 1, 1–10, 2005.

SYNTHESIS OF KAOLINITE WITH A HIGH LEVEL OF Fe^{3+} FOR Al SUBSTITUTION

Iñaki Iriarte[1,2], Sabine Petit[2], F. Javier Huertas[1,*], Saverio Fiore[3], Olivier Grauby[4], Alain Decarreau[2] and José Linares[1]

[1] Estación Experimental del Zaidín, CSIC, Profesor Albareda 1, 18008 Granada, Spain
[2] HydrASA, UMR 6532, CNRS University of Poitiers, 40 Av. du Recteur Pineau, 86022 Poitiers, France
[3] GAMLab – Institute of Methodologies for Environmental Analyses – CNR 85050 Tito Scalo (PZ), Italy
[4] CRMC2-CNRS Campus de Luminy, Case 913 Marseille Cedex, France

Abstract—Fe-rich kaolinites were synthesized at 225ºC in distilled water from gels with different Fe/Al ratios (0.15, 0.25, 0.35) and with Si/(Al + Fe) = 2. X-ray diffraction patterns of the reaction products showed that kaolinite was the only long-range crystalline phase synthesized. Analytical electron microscopy analyses of individual particles and Fourier transform infrared spectra indicated that Fe^{3+} was isomorphously incorporated into the kaolinite octahedral sheet and that tetrahedral substitution did not occur. The Fe content hosted in the synthetic kaolinites was similar to that incorporated into its corresponding starting gel. The highest Fe content in the particles reached 30 mol.% of the octahedral occupancy. Increases in the *b* parameter are proportional to increases in Fe for Al substitution. The extent of isomorphic substitution of Al by Fe is the highest ever reported for both natural and synthetic samples. At the nano-scale, there is no evidence of discontinuity in the solid-solution between the $Si_2Al_2O_7$ and $Si_2Al_{1.4}Fe_{0.6}O_7$ end-members, such as short-range disorder or clustering of Fe and Al in domains.

Key Words—Fe^{3+} substitution, Kaolinite, Solid-solution, Synthesis.

INTRODUCTION

Kaolinite is a dioctahedral 1:1 layer silicate ($Al_2Si_2O_5(OH)_4$) and was long considered to display no isomorphous substitution (Brindley *et al.*, 1986). From the 1960s onwards, however, more precise analytical techniques began to reveal that ionic substitutions are possible in both natural and synthetic samples (*e.g.* Meads and Malden, 1975; Angel *et al.*, 1975). Minor quantities of transition elements such as Fe, Ti, V, Cr and Mn may in fact be hosted in the structure of kaolinite. Magnesium is also found in natural samples and Cu kaolinite has been obtained by hydrothermal synthesis (Petit *et al.*, 1995). Among these elements, Fe is the most relevant, since in all natural kaolinites it is the most abundant impurity (*i.e.* Fe^{3+}) (Mestdagh *et al.*, 1980).

Numerous studies have dealt with the distribution of structural Fe within the kaolinite structure (Brindley *et al.*, 1986; Stone and Torres Sánchez, 1988; Delineau *et al.*, 1994; Gaite *et al.*, 1997). The most widely used tools of analysis have been the spectroscopic techniques. In the case of infrared (IR) spectroscopy, the Fe^{3+} within the octahedral sheets results in two absorption bands, one between 865 and 875 cm^{-1}, the other in the vicinity of 3600 cm^{-1}. These bands have been attributed to $\delta Fe^{3+}AlOH$ and $\nu AlFe^{3+}OH$ vibrations, respectively (Mendelovici *et al.*, 1979; Delineau *et al.*, 1994). Their existence has also been confirmed in hydrothermally synthesized Fe^{3+} kaolinite (Petit and Decarreau, 1990), and in studies of the formation of the same mineral *via* hydrothermal alteration of nontronite (Delvaux *et al.*, 1989).

Other spectroscopic techniques, such as electron paramagnetic resonance (EPR) (Meads and Malden, 1975; Muller and Calas, 1993; Gaite *et al.*, 1993; Delineau *et al.*, 1994; Balan *et al.*, 2000), ^{1}H proton magnetic resonance (Stone and Torres-Sanchez, 1988) and ^{29}Si, ^{27}Al magic angle spinning nuclear magnetic resonance (Schroeder and Pruett, 1996) have also been applied to further our understanding of ^{VI}Fe distribution in the kaolinite structure. No tetrahedral ^{IV}Fe has been proven by such techniques. On the other hand, trivalent Fe can be associated with kaolinite in nanocrystalline Fe oxide or oxy-hydroxide phases located on the surface.

The presence and distribution of Fe in natural kaolinite from diverse environments (hydrothermal, weathering and sedimentary) have been the subject of research for decades (see review in Muller *et al.*, 1995). Despite the significant amount of investigation done on kaolinite crystalchemistry, the upper limit of structural octahedral Fe^{3+} for Al substitution has yet to be determined. Natural kaolinites may contain up to 3% Fe_2O_3, which corresponds to ~0.1 ^{VI}Fe per half unit-cell. Greater quantities of Fe substitution (7% Fe_2O_3, *i.e.* ~12% of octahedral occupancy) were detected in synthetic samples by Petit and Decarreau (1990), who suggested that the octahedral Fe^{3+} could be even higher. However, to date, the Fe contents hosted in existing samples cannot be considered sufficient to define a putative kaolinite/Fe kaolinite solid-solution. It is possible that greater degrees of isomorphic substitution

* E-mail address of corresponding author:
javier.huertas@eez.csic.es
DOI: 10.1346/CCMN.2005.0530101

would make such a definition possible. To determine the continuity/discontinuity of a solid-solution at the nano-scale the following three conditions should be fulfilled: (1) a linear correlation should exist between a cell parameter and the degree of isomorphic substitution; (2) an homogeneous distribution must be observed, thus implying that the Fe and Al atoms are located evenly throughout the octahedral sheet and do not form Al kaolinite/Fe kaolinite mixed-layer clays (*i.e.* interstratified clays); and (3) a chemical-composition gradient must exist between the two end-members of the solid-solution at nano-scale.

The purpose of this paper is to present the results obtained from a set of samples synthesized for a broader study regarding the mineralogical evolution of Si_4-Al_x-Fe_y amorphous materials under varying hydrothermal environments (Iriarte, 2003). Using these samples we attempt to clarify whether the progressive incorporation of Fe into the structure makes it possible to define the Al kaolinite to (Al_xFe_{2-x}) kaolinite transition as a solid-solution. We also attempt to show that the maximum Fe content reported to date does not represent a structural limit.

MATERIALS AND METHODS

The gels used as starting materials were prepared following a slightly modified version of the method described by Decarreau *et al.* (1987). A coprecipitate of amorphous Si, Al and Fe^{3+} was obtained from a suspension by mixing two different solutions: one of Na metasilicate ($SiO_2Na_2O{\cdot}5H_2O$), the other of Al and Fe (III) chlorides ($AlCl_3{\cdot}6H_2O$ and $FeCl_3{\cdot}6H_2O$). Coprecipitation proceeds according to this overall reaction:

$$4SiO_2Na_2O + (2-x)(AlCl_3) + x(FeCl_3) + 2HCl \rightarrow (Al^{3+}_{2-x}Fe^{3+}_x)Si_4O_{11} + 8NaCl + H_2O \quad (1)$$

The first solution was prepared by dissolving Merck Na metasilicate ($SiO_2Na_2O{\cdot}5H_2O$) into distilled water up to a concentration of 0.2 mol L^{-1}. The second solution consists of Al and Fe (III) chlorides ($AlCl_3{\cdot}6H_2O$ and $FeCl_3{\cdot}6H_2O$), 0.2 mol L^{-1}, and the quantity of hydrochloric acid which is necessary to satisfy equation 1.

The chloride solution was added to the metasilicate solution while the latter was being stirred with a magnetic bar. The pH was then fixed at ~6 with hydrochloric acid. The addition of the chloride solution takes only a few minutes and the formation of the coprecipitate proceeds rapidly. However, in order to ensure the completion of the coprecipitation process, the suspension was stirred for 24 h. The final volume of suspension was 2 L.

The precipitate was recovered from the solution by centrifugation after 24 h. The solid was then washed repeatedly with distilled water and centrifuged to remove NaCl. The gel was dried at 40ºC in an oven and ground gently in an agate mortar.

Three gels were prepared using different proportions of Al and Fe^{3+} (Table 1). Chemical analyses were performed on pressed pellets by X-ray fluorescence spectrometry (XRF; Philips PW1404). Loss on ignition (LOI) was determined after solids were heated for 2 h at 1000ºC.

Subsequently, 250 mg of dry gel were aged hydrothermally in distilled water (30 mL) in teflon-lined reactors by heating at 225ºC for 60 days. Pressure inside the reactors was that of the corresponding water vapor (24.3 atm). After the ageing process, reactors were quickly cooled to prevent the precipitation of excess Si. Solids were washed repeatedly with distilled water by centrifugation, saturated overnight in $CaCl_2$ (1 mol L^{-1}) and again washed with distilled water.

The presence of alkali metals (Na) in the hydrothermal system may compensate minor layer-charge imbalances located in the 1:1 layers of kaolinite. However, the resolution of the analytical electron microscopy (AEM) is better for Ca than for Na, and thus the $CaCl_2$ solution was used to replace Na^+ with Ca^{2+} ions. The absence of Ca in the AEM spectrum of a Ca-exchanged sample indicates that no structural charge exists in the clay particle.

Solids were oven dried at 40ºC and then disaggregated and homogenized in an agate mortar. The final pH of the hydrothermal solution was measured at room temperature in the supernatant liquid recovered following the first centrifuging (Table 1).

In order to dissolve amorphous Fe oxy-hydroxides selectively, the sample obtained from the gel containing the highest Fe content (KAF54) was sequentially treated with acid oxalate and citrate-bicarbonate-dithionite (CBD) solutions (Dahlgren, 1994). To ensure complete dissolution, the extraction with acid-oxalate solution was carried out six times, and with CBD five times. The Fe, Si and Al concentrations in the extracts were determined by atomic absorption spectrometry (AAS).

Table 1. Chemical composition (wt.%), Si/Al/Fe atomic ratio of the gels used as starting materials, corresponding sample and initial and final pH of the hydrothermal solution.

Gel	SiO_2	Al_2O_3	Fe_2O_3	Na_2O	LOI	Sum	Si/Al/Fe	Sample	$pH_{initial}$ (±0.05)	pH_{final} (±0.05)
GAF28	55.00	20.87	5.10	3.97	15.09	100.08	4/1.79/0.28	KAF28	6.69	5.09
GAF42	54.38	18.62	7.55	4.77	15.50	100.88	4/1.61/0.42	KAF42	6.73	4.97
GAF54	54.28	17.41	9.81	4.04	14.42	100.05	4/1.51/0.54	KAF54	6.74	5.02

K_2O, P_2O_5, TiO_2 and MnO were <0.01%. LOI: loss on ignition at 1000ºC.

https://doi.org/10.1346/CCMN.2005.0530101 Published online by Cambridge University Press

Gels and samples were examined by X-ray diffraction (XRD) using a Siemens D501 diffractometer (CuKα radiation, 40 kV, 30 mA) equipped with an XRF detector (Si-Li diode). X-ray powder diffraction patterns of bulk samples were recorded using random orientation mounts, accurate peak positions being obtained by adding a LiF internal standard. The 220 reflection of LiF was used to calibrate the 060 reflection of clay minerals. Oriented clay mineral aggregates were prepared by dispersing the sample with an ultrasonic probe and pipetting the suspension onto a glass slide. The possible occurrence of swelling phases was tested by comparing samples under air-dried (AD) conditions with subsequent ethylene glycol (EG) solvation.

Clay-particle morphology was observed using scanning electron microscopy (SEM) and transmission electron microscopy (TEM). The SEM observations were carried out using two microscopes: a W-filament microscope and a field emission apparatus (FE-SEM). The conventional SEM was a Cambridge Stereoscan S360 working at 20 kV, 100–500 pA and equipped with an energy dispersive X-ray spectrometer (Oxford Link with a Ge detector). The FE-SEM was a LEO 1530 operating at 1–2 kV, an aperture of 30 μm and a working distance of 5–6 mm. The LEO 1530 was coupled with a LINK 400 EDS. Samples were dispersed in water by a weak ultrasonic treatment and a drop of suspension was left to dry on a carbon stub. The samples were carbon coated.

The TEM observations were performed using a Jeol 2000 FX microscope working at 200 kV and equipped with a Tracor TN-5502 energy dispersive X-ray spectrometer. Samples were suspended in water and a drop of the suspension was left to dry on a carbon-coated Cu microgrid. Analytical electron microscopy was operated in the fixed-electron-beam mode with the objective aperture removed. Beam diameter was 200–400 Å and beam current was 1.2 nA. Counting time was 100 s. Quantitative calibration was carried out using layer silicate standards and the method described by Cliff and Lorimer (1975).

Differential thermal analysis (DTA) and thermogravimetry (TG) were carried out using a Netzsch STA 409EP simultaneous thermal analyzer, under the following conditions: 15 mg of sample; Al_2O_3 as reference material; temperature range from 25 to 1020ºC; heating rate of 10ºC/min; and air atmosphere. Temperature limits for each reaction were established using the DTA, TG and the first derivative of the TG (DTG) curves.

Fourier transform infrared (FTIR) spectra were recorded in transmission mode in the 4000–400 cm^{-1} range using a Nicolet 510 FTIR spectrometer with a resolution of 4 cm^{-1}. Samples were prepared in KBr pressed pellets by diluting 1 mg of sample in 150 mg of dried KBr. The pellets were heated overnight at 120ºC before analysis.

RESULTS

X-ray diffraction

The starting gels exhibited no X-ray crystalline phases (data not shown). Powder XRD patterns of the synthesis products revealed that kaolinite is the only crystalline phase present (Figure 1). The amount of Fe^{3+} in the synthetic sample did not modify the reflection positions but contributed to reducing their relative intensities. As kaolinite Fe content rises, the intensities and resolutions of the $110-1\bar{1}0$ and $1\bar{1}1-1\bar{1}\bar{1}$ peaks, as well as the Hinckley crystallinity index (Hinckley, 1963) decrease (Table 2). The average coherent scattering domain (ACSD) along the b^* and c^* axes, calculated using the Scherrer equation (Guinier, 1956) with the 060 and 001 reflections, respectively, showed that crystal sizes average ~190 Å along the c^* axis and 310 Å along the b^* axis. This is slightly higher than those reported

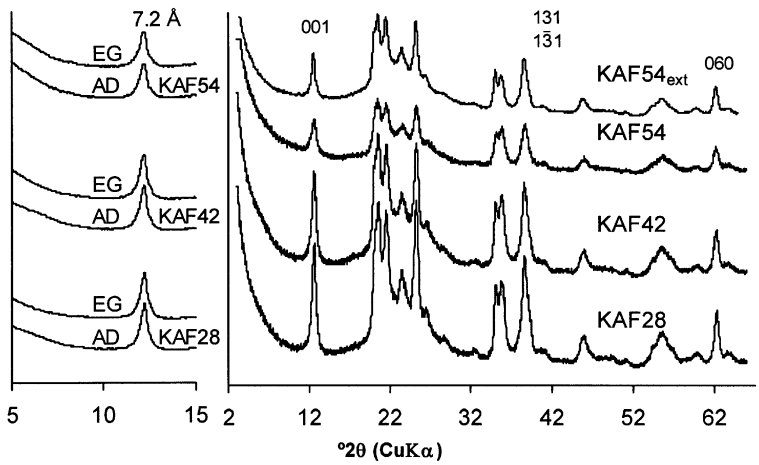

Figure 1. XRD patterns of synthetic kaolinites. KAF54$_{ext}$ corresponds to sample KAF54 after extraction treatment with acid oxalate and citrate-bicarbonate-dithionite solutions. AD: air dried; EG: solvated with ethylene glycol.

https://doi.org/10.1346/CCMN.2005.0530101 Published online by Cambridge University Press

Table 2. Crystallographic XRD parameters of synthetic kaolinites.

Sample	*b* (Å) (±0.003)	Hinckley Index	ACSD[1] (Å) (Number of unit-cells) 001	060
KAF28	8.960	0.75	196 (28)	304 (34)
KAF42	8.976	0.70	187 (27)	312 (35)
KAF54	8.984	0.54	179 (26)	324 (36)
Natural[2]	8.946			
Synthetic Al kaolinite[3]		0.91	260 (37)	236 (26)

[1] ACSD: Average coherent scattering domain; number of unit-cells between brackets. [2] Bailey (1980). [3] Synthetic Al kaolinite to 220ºC, initial pH = 6.5, final pH = 6.0 (Fialips *et al.*, 2000)

for synthetic Al kaolinite obtained under similar experimental conditions (Fialips *et al.*, 2000). As the Fe content increases, a slight trend was observed for stacked layers to decrease and for crystal sizes to become larger in the *b* direction (Table 2).

The 131 and $1\bar{3}1$ reflections are not resolved, thus revealing the monoclinic character of these kaolinites (Plançon and Tchoubar, 1977; Brindley and Porter, 1978). The 060 reflection of the three samples fits well with a unimodal Gaussian curve, indicating that there was no demixing between the Al kaolinite and Fe kaolinite scattering domains. The *b* dimensions are 0.014–0.038 Å larger than those of pure Al kaolinite (Bailey, 1980). Furthermore, these values increase with the Fe content of the starting gel (Table 2), in agreement with the progressive incorporation of Fe into the kaolinite structure and the difference in ionic radius of Fe (0.64 Å) *vs.* Al (0.51 Å) in octahedral coordination.

Kaolinite shows a band at ~1.5 Å, often labeled as 060, which is a convolution of three reflections: 060 (d = 1.4901 Å, intensity 10.0), $\bar{3}\bar{3}1$ (d = 1.4899 Å, intensity 10.3) and $\bar{3}31$ (d = 1.4868 Å, intensity 10.3) (Collins and Catlow, 1991). No preferred orientation can separate one diffraction peak from the others. Rieder *et al.* (1992) argued that a systematic error is introduced by using the d spacing of the 1.5 Å band to estimate the *b* parameter in muscovites. However, due to the very small difference in d spacing, no serious error is introduced if the measure of the composite peak is converted to *b*. Furthermore, this line of reasoning does not invalidate the correlation between d spacing of the 1.5 Å band and the (Fe+Mg) content in muscovites. Assuming that this argument can also be applied to kaolinites, we will use this estimation of the *b* parameter to correlate cell dimensions and Fe content. A true *b* parameter should be calculated by unit-cell refinement.

Differential thermal analysis and thermogravimetry (DTA-TG)

The DTA-TG curves of the samples exhibited three endothermic events and one exothermic one (Figure 2). The first endothermic event (~83ºC) corresponds to the loss of adsorbed water. The second weak peak occurred at 291ºC and, as shown later, may be associated with water molecules strongly adsorbed to kaolinite, hydroxyls of residual gel, or FeOOH and AlOOH nanocrystals. The third peak occurs in the range 497–512ºC and is attributed to the dehydroxylation of kaolinite (Mackenzie, 1970). The presence of structural Fe^{3+} in the kaolinite lowers the dehydroxylation and exothermic event temperatures. Similar decreases in these temperatures were reported for synthetic Cu kaolinites (Petit *et al.*, 1995). The dehydroxylation peak area and the weight loss associated with this event were used to estimate the quantity of kaolinite formed; the amount decreased with increase in the Fe content of the starting material (Table 3).

The chemistry of the starting gels has excess silica of ~30% compared to the chemistry of kaolinite with a structural formula $(Al_{2-x}Fe_x)Si_2O_5(OH)_4$. The kaolinite yield could reach a maximum of 70%. However, kaolinite content after the hydrothermal treatment, calculated by TG analysis, was ~50% (Table 3). The remaining 50% of solid corresponds to gel or other X-ray

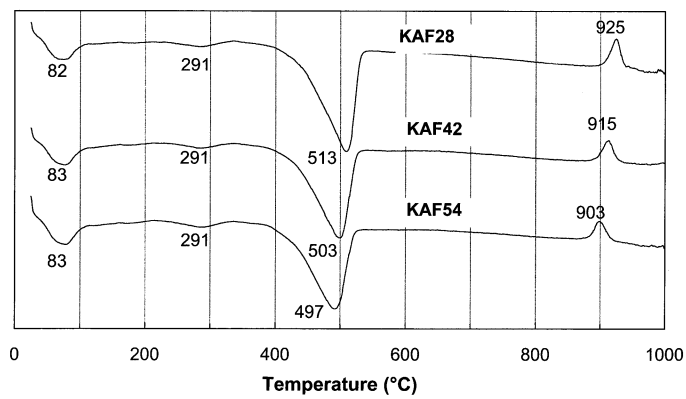

Figure 2. DTA curves of synthetic kaolinites.

https://doi.org/10.1346/CCMN.2005.0530101 Published online by Cambridge University Press

Table 3. Summary of data from DTA and TG curves for the studied samples.

Sample	Weight loss (%)			Kaolinite %[1]	Area[2]
	25–130ºC	400–550ºC	25–1020ºC		
KAF28	3.36	6.72	11.76	48	664
KAF42	2.47	6.41	11.55	45	592
KAF54	3.69	6.31	11.83	41	559

[1] Estimated on exothermic event of dehydroxylation and assuming 14% (wt.%) OH^- in kaolinite
[2] Area of the DTA dehydroxylation peak (arbitrary units)

amorphous material such as AlOOH or FeOOH, which break down at ~290ºC.

Electron microscopy

Samples examined with a conventional SEM (W filament) had grains ranging from several to tens of μm in size. Grains generally displayed a porous and spongy texture. When the samples were examined using a FE-SEM apparatus, they exhibited different morphological features from those described for natural kaolinite. Sample KAF28, synthesized from the gel with the lowest Fe content, showed kaolinite particles arranged in a honeycomb-like structure with high porosity (Figure 3a). Most of the particles form aggregates of flat particles with needle terminations and connected by thin 'membranes' producing a flake-like appearance. Lath or elongated crystals are also present. Sample KAF42 (from the gel with intermediate Fe content; Figure 3b) contained a larger amount of lath-shape particles than the previous one. These lath-like particles are isolated or form aggregates. The isolated laths are mainly observed on the unreacted gel grains and on grains under transformation. Gel grains exhibit a texture resembling stacks of layers. The aggregates are more compact than those that appear in sample KAF28. Very small particles are frequently observed on the grain surface of these samples. Sample KAF54, the richest in Fe, displays a highly compact structure, formed by small curved or bent layers that give rise to large surfaces with honeycomb structures (Figure 3c). This texture bears a striking resemblance to that of smectites. However, EDS chemical data of the plates arranged in the honeycomb structures always correspond to Fe kaolinite, and not to 2:1 clays. Grain surfaces are completely free of fine matter and no isolated particles are observed.

Individual particles were also studied by TEM-AEM. Three main morphologies were observed: laths, plates and thin and curly hair-like particles. The hair-like particles (Figure 4a) consist of thin crystals, 100–300 nm long and 5–10 nm thick. Selected area electron diffraction (SAED) could not be obtained because of instability under the beam. The SAED imaging revealed that some of these particles consist of kaolinite crystals which are curved on the *ab* plane. Platy morphologies (Figure 4b) are grouped in small aggregates of crystals (50–100 nm in diameter). They frequently exhibit hexagonal or pseudohexagonal outlines and SAED patterns of (*hkl*) planes. However, many

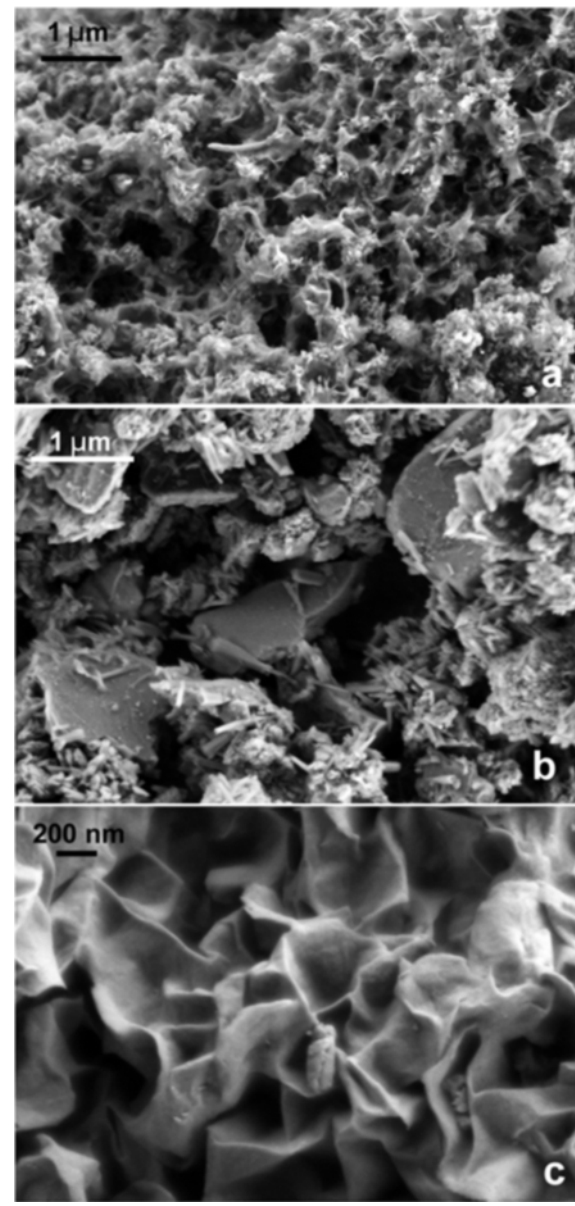

Figure 3. FE-SEM images of synthetic Fe kaolinites: (a) KAF28; (b) KAF42; and (c) KAF54.

https://doi.org/10.1346/CCMN.2005.0530101 Published online by Cambridge University Press

hexagonal particles do not produce electron diffraction patterns, probably because there are very few stacked kaolinite layers and/or the particle becomes amorphous under the electron beam. Lath-like crystals, in some cases with hexagonal termination, form aggregates together with residual gel or kaolinite plates (Figure 4c). They correspond to the longest particles, which are ~50 nm wide and 300 nm long. These thin elongated particles become amorphous under the electron beam. No other euhedral phases were observed and spherical kaolinite habits were not detected.

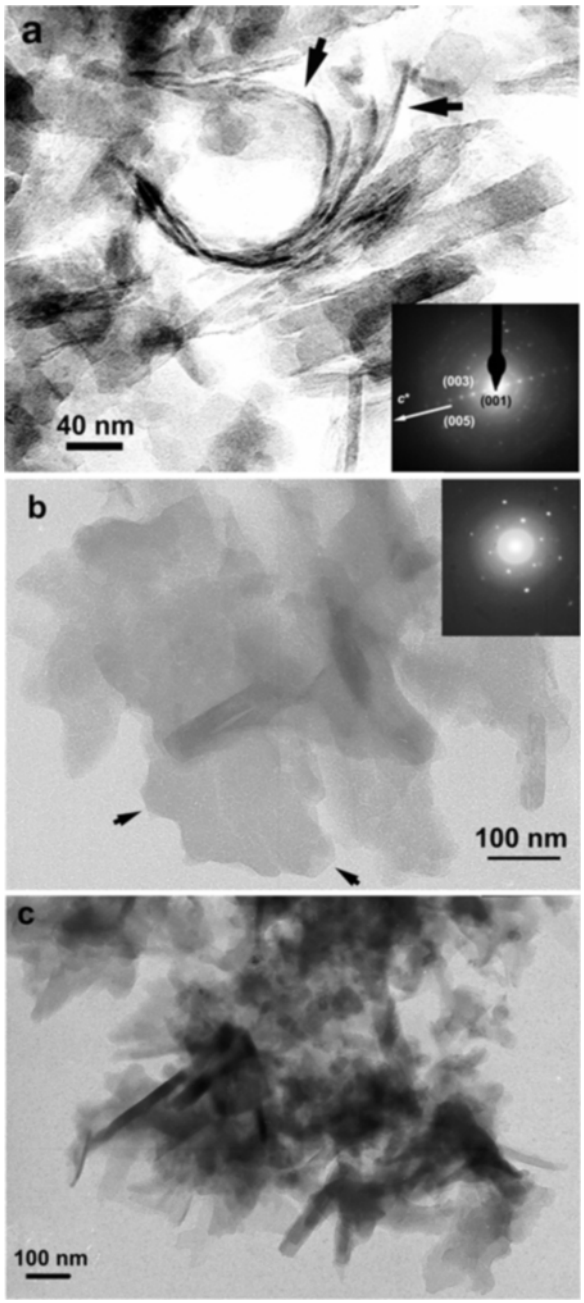

Figure 4. TEM images of synthetic Fe kaolinite particles: (a) hair-like kaolinite (arrows) crystals (KAF54) and SAED pattern; (b) particles with platy morphology and hexagonal outline (arrow) of KAF28 and their SAED pattern; and (c) aggregates of lath-like crystals and amorphous material (KAF54).

The AEM chemical analyses were performed on isolated particles (Table 4). Quantitative analyses of laths and plates show several important features: (1) neither Ca nor Na was detected in kaolinite particles, indicating no charge compensation and thus no smectite and no heterovalent substitutions; (2) kaolinite crystals containing only Al or only Fe in the octahedral sheet were never detected; and (3) the average Al/Fe ratio in the analyzed particles is similar to that in the starting gel. These data indicate that the gels were transformed into kaolinites with the same Fe/Al stoichiometry.

Fe extraction

Iron extraction procedures were performed only on the sample which was richest in Fe (KAF54). The aim of this treatment was to determine the possible existence of Fe phases not detected by XRD or TEM. The acid-oxalate solutions dissolve mainly Al, whereas the CBD extracts mainly Fe and Si. In both cases, the extraction

Table 4. Al and Fe content in the octahedral sheet of kaolinite particles analyzed by AEM. There is no tetrahedral substitution and thus Si = 2 (see text).

Sample	^{VI}Al	^{VI}Fe
KAF54	1.41	0.59
	1.38	0.62
	1.42	0.58
	1.52	0.48
	1.57	0.43
	1.62	0.38
	1.50	0.50
	1.50	0.50
Average	1.49	0.51
St. dev.	0.08	0.08
KAF42	1.61	1.39
	1.55	0.45
	1.59	0.41
	1.63	0.37
	1.57	0.43
	1.60	0.40
	1.57	0.43
Average	1.59	0.41
St. dev.	0.03	0.03
KAF28	1.75	0.25
	1.72	0.28
	1.68	0.32
	1.71	0.29
	1.64	0.36
	1.63	0.37
	1.61	0.39
Average	1.68	0.32
St. dev.	0.05	0.05

https://doi.org/10.1346/CCMN.2005.0530101 Published online by Cambridge University Press

occurred principally during the first step and the total amount of solid dissolved is negligible, corresponding to <0.2%, 0.03% and 0.01% of total Fe, Al and Si, respectively (Table 5). The ratio of the extracted cations did not match the stoichiometry of the synthetic Fe kaolinite, suggesting that dissolved Al and Fe do not only come from kaolinite.

The XRD powder pattern recorded after extraction (Figure 1) shows a notable improvement in the resolution of *hkl* reflections. The average coherent scattering domain also increases, as indicated by a narrower 001 reflection. The monoclinic character of kaolinite is preserved after the treatments. It can be concluded that the treatments dissolved a small quantity of the gel and poorly ordered kaolinites, thus inducing an increase in crystallinity both along the *b** (376 Å) and *c** (280 Å) dimensions.

Table 5. Concentration of Si, Al and Fe in the solution after sequential extraction with acid oxalate solution (T_1–T_6) and CBD solution (T_7–T_{11}).

	Stage	Si (mmol L^{-1})	Al (mmol L^{-1})	Fe (mmol L^{-1})
Acid-oxalate	T_1	0.04	0.19	0.01
	T_2	0.04	0.03	b.d.l.
	T_3	0.04	0.01	b.d.l.
	T_4	0.03	b.d.l.	b.d.l.
	T_5	0.04	b.d.l.	b.d.l.
	T_6	0.04	b.d.l.	b.d.l.
Total	(T_1–T_6)	0.23	0.23	0.01
CBD	T_7	0.19	0.28	2.29
	T_8	0.13	0.19	0.59
	T_9	0.16	0.15	0.18
	T_{10}	0.14	0.10	0.04
	T_{11}	0.13	0.10	0.01
Total	(T_7–T_{11})	0.75	0.82	3.11

b.d.l.: below detection limit

Infrared spectroscopy

In the OH-stretching region (Figure 5a), a first group of four bands (3692, 3669, 3654 and 3620 cm^{-1}, labelled ν_1, ν_2, ν_3 and ν_4, respectively (Brindley *et al.*, 1986)) corresponding to νAl_2OH vibrations is characteristic of kaolinite. The three higher-frequency bands are due to surface OHs, whereas the ν_4 band originates from the inner OH (Farmer, 1974).

Another absorption band is observed at 3598 cm^{-1} in the Fe kaolinites and has been reported in natural and synthetic Fe-substituted kaolinites, being assigned to $\nu AlFe^{3+}OH$ (Mendelovici *et al.*, 1979; Petit and Decarreau, 1990). A small band also occurs at 3430 cm^{-1} which has been observed in natural disordered kaolinite (Delineau *et al.*, 1994; Tomura *et al.*, 1985) and in synthetic kaolinites (De Kimpe *et al.*, 1981; Martin *et al.*, 1998). This band still appears after extraction of amorphous phases and after pellet disks have been heated at 100, 200 and 250ºC. In contrast, it is no longer present following heating of the pellet disks at 300ºC. As is also suggested by the endothermic event recorded at 291ºC in the DTA curves, this band may be accounted for by the presence of strongly adsorbed

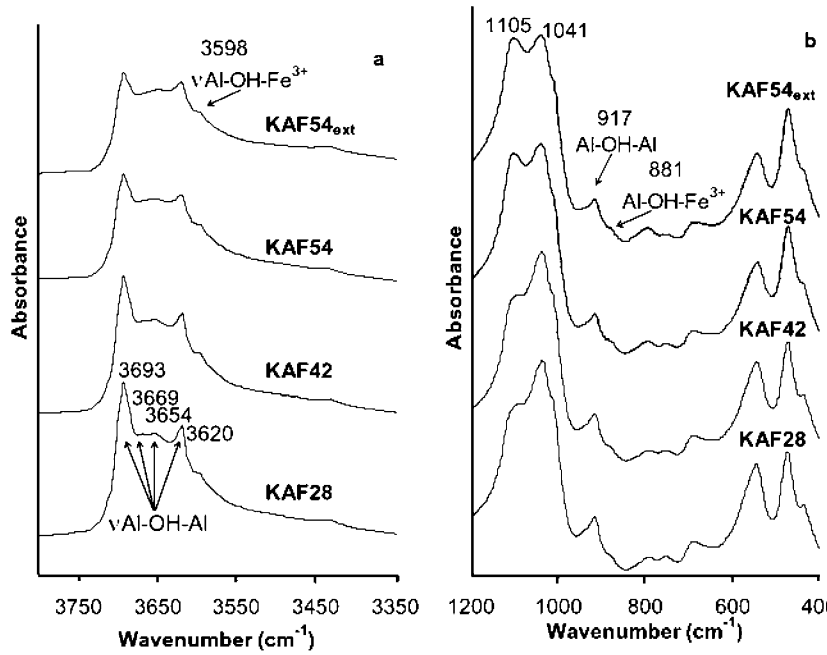

Figure 5. FTIR spectra in: (a) the OH-stretching region and (b) the OH-bending region of the Fe^{3+}-substituted kaolinites under study. KBr pellets were dried at 120ºC overnight before recording the spectra. Spectra of the sample KAF54 after extraction treatment are also shown ($KAF54_{ext}$).

https://doi.org/10.1346/CCMN.2005.0530101 Published online by Cambridge University Press

water. Furthermore, this band might also correspond to gibbsite-like or goethite-like nano-crystalline phases.

In the 1200–400 cm^{-1} region (Figure 5b), all of the bands observed are due to kaolinite, except that at 1105 cm^{-1} which corresponds to silica (database FDM FTIR spectra ©2000) derived from its release during the transformation of the gel into kaolinite; its intensity increases with the Fe content of the sample.

The band at 917 cm^{-1} corresponds to δAl_2OH vibrations, whereas the weak band, centered at 881 cm^{-1}, is attributed to δFeAlOH (Mendelovici *et al.*, 1979; Petit and Decarreau, 1990). Figure 6 shows an enlarged view of the OH-bending vibrations region in which the spectra have been normalized with the δAl_2OH band. It can be observed that the intensity of the δFeAlOH band increases with the Fe content of the samples.

No significant change is exhibited by the FTIR spectrum of the sample after extraction treatment (Figure 5a,b). The characteristic bands of AlFeOH vibrations are still present, which clearly shows that Fe is a component of the kaolinite structure and that the samples are authentic Fe-substituted kaolinites.

DISCUSSION AND CONCLUSIONS

Si-rich starting materials can be used to improve crystallinity and yield in kaolinite synthesis (Rodrique *et al.*, 1972; De Kimpe *et al.*, 1981; Huertas *et al.*, 1999). Previous research regarding the hydrothermal synthesis of Fe^{3+} kaolinite has produced Fe-substituted kaolinite with smaller amounts of Fe than those of the starting material (Calvert, 1981). In contrast, the present work shows, using Si-rich starting materials, that the kaolinite particle Fe content is close to that in the starting gel. The resulting kaolinite crystals are homogeneous in composition and no other minerals were detected. Nevertheless, an increase in the crystalline disorder is observed as the Fe content increases. We suggest that this is due to the presence of small quantities of X-ray amorphous materials, as is supported by the observation that the Fe extraction process produces an increase in both crystallinity and crystal size (Figure 1).

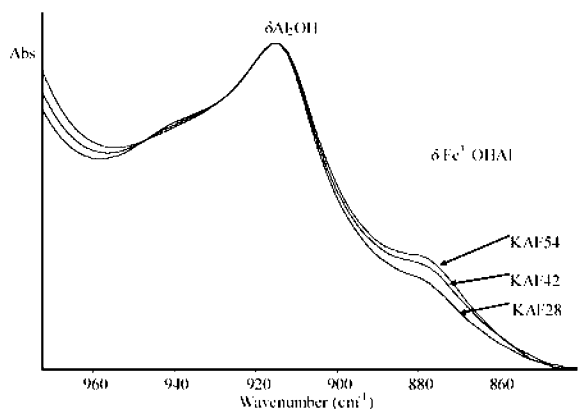

Figure 6. Spectral window between 1000 and 800 cm^{-1} using the δAl_2OH band to normalize the spectra.

The increase of the d_{060} spacing is also consistent with the progressive incorporation of Fe into the octahedral sheet. The *b* parameter displays a linear dependence with the Fe substitution (Figure 7) following:

$$b = 8.946 + 0.074x \quad (2)$$

where *x* is the number of Fe^{3+} atoms that substitute those of Al per half unit-cell. The slope is similar to the 0.075 Å value measured by Russell and Clark (1978) for Fe^{3+} in octahedral sites of nontronites. Assuming that this linear relationship could be extended to a pure Fe end-member, a value of 9.09 Å would be expected for the *b* parameter of a pure Fe kaolinite with no tetrahedral substitution ($x = 2$). This value is similar to that measured for dioctahedral 2:1 Fe end-members, nontronite (9.11–9.14 Å, WWW-Mincryst database, 2003) and ferripyrophyllite (9.10 Å, Gaines *et al.*, 1997), while it is smaller than that measured for trioctahedral 1:1 phyllosilicates (*i.e.* chrysotile, 9.25 Å) (Bailey, 1980).

Iron substitution of Al in kaolinite is supported by the occurrence of νAlFeOH and δAlFeOH bands in IR spectra. In the bending region, the absorbance of the δAlOHFe band increases relative to the absorbance of the δAl_2OH bands (Figure 6) in accordance with the chemical compositions of the particles. On the other hand, as the Fe content of samples increases, no clear increase in the νAlFeOH band is observed in the stretching region and Fe_2OH bands do not appear (Figure 5a). Only one νAlFeOH band has been reported to occur at 3598 cm^{-1} (see above). However, it is conceivable that at least two νAlFeOH bands exist corresponding to vibrations of the internal OH and

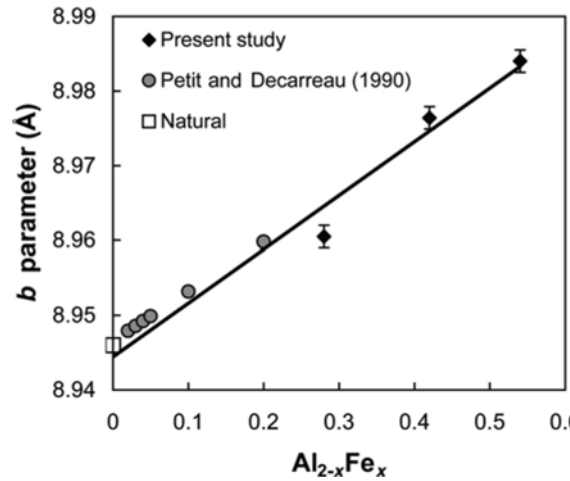

Figure 7. Relationships between ^{VI}Fe substitution per half unit-cell and *b* parameter (Å) calculated from 060 reflection in XRD patterns. Natural kaolinite (Bailey, 1980) and data from Petit and Decarreau (1990) are also included.

https://doi.org/10.1346/CCMN.2005.0530101 Published online by Cambridge University Press

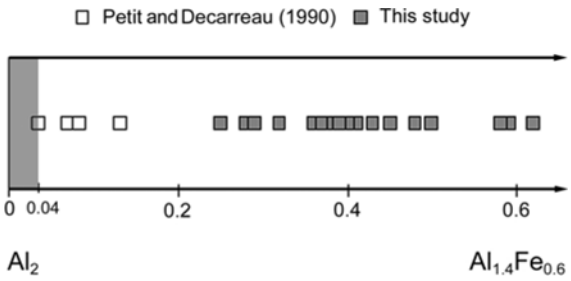

Figure 8. Composition of the octahedral sheet of isolated kaolinite particles by AEM. Dark area on the left corresponds to natural kaolinites. Data from Petit and Decarreau (1990) are also included (open symbol).

surface OH. One hypothesis is that several νAlFeOH bands exist and that only one of them is clearly observed at 3598 cm^{-1}, while the other(s) may be overlapped by the $n$$Al_2OH$ bands. This may explain why the resolution of ν_1, ν_2, ν_3 and ν_4 varies with the Fe content and why the absorbance of the νAlOHFe does not display the same variation as the δAlOHFe band. Further spectroscopic studies of Fe kaolinite will be required to confirm this hypothesis.

Particle chemical compositions were homogeneous, without exsolution into enriched or pure Al and Fe end-members. The 060 reflection fits well with a unimodal Gaussian curve, indicating that the samples do not consist of particles, layers or coherent domains of pure Al kaolinite and Fe kaolinite.

The absence of Ca in the TEM-AEM analyses of Ca-saturated individual particles shows that tetrahedral substitution does not occur in kaolinite and that all the Fe quantified is therefore incorporated into the octahedral sheet. Relative octahedral compositions per half unit-cell of natural and synthesized kaolinite particles are shown in Figure 8. In natural samples, x ranges from 0 to 0.04. In synthetic particles, Petit and Decarreau (1990) measured x = 0.2. In this study, the nano-scale measurements make it possible for the first time to characterize Fe-substituted kaolinites whose ^{VI}Fe values are in the range $0.25 < x < 0.60$.

In summary, a linear correlation is observed between the b parameter and the Fe substitution, the Fe and Al coexist in the same octahedral sheet and a chemical-composition gradient exists between $Al_2Si_2O_7$ and $Al_{1.4}Fe_{0.6}Si_2O_7$. Consequently, the Al kaolinite–Fe kaolinite series behaves as a solid-solution within the compositional range explored and no evidence exists to date that the maximum value obtained (x = 0.6) represents a structural limit. It is possible that the application of other spectroscopic techniques (*e.g.* ^1H, ^{27}Al and ^{29}Si nuclear magnetic resonance, and electron paramagnetic resonance) would improve the characterization of Fe kaolinites. Further investigation will thus be required in order to deepen our understanding of the extension of the Al-Fe kaolinite solid-solution.

ACKNOWLEDGMENTS

This research was financed by DGES project PB97-1215 and by an FPI grant from the Spanish Ministerio de Ciencia y Tecnología. We would like to thank M.J. Civantos and C. Fontaine for their technical assistance. We are also grateful to Assing Spa (Italy) for the use of their FE-SEM microscope. The XRF analyses were performed at the Centro de Instrumentación Científica, University of Granada. The manuscript benefited from corrections and suggestions by P.A. Schroeder and D.G. Schulze. Editing of the original English manuscript was done by Marc John Bettini.

REFERENCES

Angel, B.R., Richards, K. and Jones, J.P.E. (1975) The synthesis, morphology, and general properties of kaolinites specifically doped with metallic ions, and defects generated by irradiation. *Proceedings of the International Clay Conference 1975.* Applied Publishing Ltd. pp. 297–304.

Bailey, S.W. (1980) Structures of layer silicates. Pp. 1–123 in: *Crystal Structures of Clay Minerals and their X-ray Identification* (G.W. Brindley and G. Brown, editors). Monograph No. 5, Mineralogical Society, London.

Balan, E., Allard, T., Boizot, B., Morin, G. and Muller, J.P. (2000) Quantitative measurement of paramagnetic Fe^{3+} in kaolinite. *Clays and Clay Minerals*, **48**, 439–445.

Brindley, G.W. and Porter, A.R.D. (1978) Occurrence of dickite in Jamaica-ordered and disordered varieties. *American Mineralogist*, **63**, 554–562.

Brindley, G.W., Chih-Chun Kao, Harrison, J.L., Lipsicas, M. and Raythatha, R. (1986) Relation between structural disorder and other characteristics of kaolinites and dickites. *Clays and Clay Minerals*, **34**, 239–249.

Calvert, C.S. (1981) *Chemistry and mineralogy of iron substituted kaolinite in natural and synthetic systems*. Michigan University Microfilms International, Ann Arbor, Michigan, 224 pp.

Cliff, G. and Lorimer, G.W. (1975) The quantitative analysis of thin specimens. *Journal of Microscopy*, **103**, 203–207.

Collins, D.R. and Catlow, C.R.A. (1991) Energy minimization hydrogen-atom positions at kaolinite. *Acta Crystallographica*, **B47**, 678–682.

Dahlgren, R.A. (1994) Quantification of allophane and imogolite. Pp. 430–451 in: *Quantitative Methods in Soil Mineralogy* (J.E. Amonette and L.W. Zelazny, editors). SSSA Miscellaneous Publications, Soil Science Society of America.

Decarreau, A., Bonnin, D., Badaut-Trauth, D., Couty, R. and Kaiser, P. (1987) Synthesis and crystallogenesis of ferric smectite by evolution of Si-Fe coprecipitates in oxidising conditions. *Clay Minerals*, **22**, 207–223.

De Kimpe, C.R., Kodama, H. and Rivard, R. (1981) Hydrothermal formation of kaolinite-like product from noncrystalline aluminosiliate gels. *Clays and Clay Minerals*, **29**, 446–450.

Delineau, T., Allard, T., Muller, J.P., Barrès, O., Yvon, J. and Cases, J.M. (1994) FTIR reflectance vs. EPR studies of structural iron in kaolinites. *Clays and Clay Minerals*, **42**, 308–320.

Delvaux, B., Mestdagh, M.M., Vielvoye, L. and Herbillon, A.J. (1989) Spectroscopic study of the nontronite→kaolinite hydrothermal transformation. Application to a weathering sequence Fe-smectite→kaolinite. *Clay Minerals*, **24**, 617–632.

Farmer, V.C. (1974) The layer silicates. Pp. 331–365 in: *The Infrared Spectra of Minerals* (V.C. Farmer, editor). Monograph **4**, Mineralogical Society, London,.

Fialips, C.I., Petit, S., Decarreau, A. and Beaufort, D. (2000) Influence of synthesis pH on kaolinite crystallinity and surface properties. *Clays and Clay Minerals*, **48**, 173–184.

Gaines, R.V., Skinner, H.C.W., Foord, E.E., Mason, B. and Rosenzweig, A. (1997) *Dana's New Mineralogy*. John Wiley & Sons, Inc., New York, 1819 pp.

Gaite, J.M., Ermakoff, P. and Muller, J.P. (1993) Characterization and origin of two Fe^{3+} EPR spectra in kaolinite. *Physics and Chemistry of Minerals*, **20**, 242–247.

Gaite, J.M., Ermakoff, P., Allard, Th. and Muller J.P. (1997) Paramagnetic Fe^{3+}: A sensitive probe for disorder in kaolinite. *Clays and Clay Minerals*, **45**, 496–505.

Guinier, A. (1956) Diffraction par les cristaux de très petite taille. Pp. 462–465 in: *Théorie et Technique de la Radiocristallographie* (A. Guinier, editor). Dunod, Paris.

Hinckley, D.N. (1963) Variability in crystallinity values among the kaolin deposits of the coastal plain of Georgia and South Carolina. *Clays and Clay Minerals*, **11**, 229–235.

Huertas, F.J., Fiore, S., Huertas, F. and Linares, J. (1999) Experimental study of hydrothermal formation of kaolinite. *Chemical Geology*, **156**, 171–190.

Iriarte, I. (2003) Formación de minerales de la arcilla en el sistema SiO_2-Al_2O_3-Fe_2O_3-MgO-Na_2O-H_2O entre 150 y 225ºC. PhD thesis, University of Granada, Spain.

Mackenzie, R.C. (1970) Simple phyllosilicates based on gibbsite- and brucite-like sheets. Pp. 497–551 in: *Differential Thermal Analysis* (R.C. Mackenzie, editor). Academic Press, London.

Martin, F., Petit, S., Decarreau, A., Ildefonse, P., Grauby, O., Beziat, D., Parseval, P. and Noack, Y. (1998) Ga/Al substitution in synthetic kaolinites and smectites. *Clay Minerals*, **33**, 231–241.

Meads, R.E. and Malden, P.S. (1975) Electron-spin resonance in natural kaolinites containing Fe^{3+} and other transition metal ions. *Clay Minerals*, **10**, 313–345.

Mendelovici, E., Yariv, S.H. and Villalva, R. (1979) Iron-bearing kaolinite in Venezuelan laterites. I. Infrared spectroscopy and chemical dissolution evidence. *Clay Minerals*, **14**, 323–331.

Mestdagh, M.M., Vielvoye, L. and Herbillon, A.J. (1980) Iron in kaolinites: II. The relationship between kaolinite crystallinity and iron content. *Clay Minerals*, **15**, 1–13.

Muller, J.P. and Calas, G. (1993) Genetic significance of paramagnetic centers in kaolinites. Pp. 261–289 in: *Keller Kaolin 90 Symposium* (M. Bundy, H.H. Murray and C.C. Harvey, editors). The Clay Minerals Society, Boulder, Colorado.

Muller, J.P., Manceau, A., Calas, G., Allard, T., Ildefonse, P. and Hazemann, J.L. (1995) Crystal chemistry of kaolinite and Fe-Mn oxides: relation with formation conditions of low temperature systems. *American Journal of Sciences*, **295**, 1115–1155.

Petit, S. and Decarreau, A. (1990) Hydrothermal (200ºC) synthesis and crystal chemistry of iron-rich kaolinites. *Clay Minerals*, **25**, 181–196.

Petit, S., Decarreau, A., Mosser, C., Ehret, G. and Grauby, O. (1995) Hydrothermal synthesis (250ºC) of copper-substituted kaolinites. *Clays and Clay Minerals*, **43**, 482–494.

Plançon, A. and Tchoubar, C. (1977) Determination of structural defects in phyllosilicates by X-ray powder diffraction – II. Nature and proportion of defects in natural kaolinites. *Clays and Clay Minerals*, **25**, 436–450.

Rieder, M., Guidotti, C.V., Sassi, F.P. and Weiss, Z. (1992) Muscovites: d_{060} versus $d_{33\bar{1},060}$ spacing: its use for geobarometric purposes. *European Journal Mineralogy*, **4**, 843–845.

Rodrique, L., Poncelet, G. and Herbillon, A. (1972) Importance of the silica subtraction process during the hydrothermal kaolinitization of amorphous silico-aluminas. *Proceedings of the International Clay Conference, Madrid*, pp. 853–885.

Russell, J.D. and Clark, D.R. (1978) The effect of Fe for Si substitution on the *b* dimension of nontronite. *Clay Minerals*, **13**, 133–137.

Schroeder, P.A. and Pruett, R.J. (1996) Fe ordering in kaolinite: Insights from ^{29}Si and ^{27}Al MAS NMR spectroscopy. *American Mineralogist*, **81**, 26–38.

Stone, W.E.E. and Torres Sánchez, R.M. (1988) Nuclear magnetic resonance spectroscopy applied to minerals. Part 6. Structural iron in kaolinite as viewed by proton magnetic resonance. *Journal of the Chemical Society, Faraday Transactions I*, **84**, 117–132.

Tomura, S., Shibasaki, Y., Mizuta, H. and Kitamura, M. (1985) Growth conditions and genesis of spherical and platy kaolinite. *Clays and Clay Minerals*, **33**, 200–206.

WWW-Mincryst (2003) Crystallographic Database for Minerals and their Structural Analogues. http://database.iem.ac.ru/mincryst/

(*Received 5 April 2004; revised 18 October 2004; Ms. 898*)